OL Organic Letters

pubs.acs.org/OrgLett Letter

Distahlianins A–C: Architecturally Diverse Cadinane-Type Sesquiterpenoid Dimers from *Stahlianthus involucratus*

Kai-Long Ji,* Yu-Han Chen, Qin-Qin Song, Xi-Yu Zheng, Peng Sun, Jian-Mei Lu, Gang Liang,* and Yao-Yue Fan*

Cite This: *Org. Lett.* 2025, 27, 10843–10848 Read Online

ACCESS | Metrics & More | Article Recommendations | Supporting Information

ABSTRACT: Three architecturally novel cadinane sesquiterpenoid dimers, distahlianins A–C (**1**–**3**), were isolated from *Stahlianthus involucratus*. Compounds **1** and **2** are characterized by an unusual 5,6-spirocyclic scaffold annulated with oxygenated heterocycles to form intricate 6/6/5/6/6/6 and 6/6/5/5/6/6 hexacyclic frameworks, respectively. Compound **3** features a unique dimeric skeleton formed by two monomeric units bridged through a cyclopentane ring. Intriguingly, structural analysis revealed a unique C14 methyl migration (C-9→C-8) in the left monomer unit of **3**, representing a new cadinane skeletal feature. Compound **3** exhibited potent lipid-lowering activity, with mechanistic evidence pointing to lipogenesis suppression.

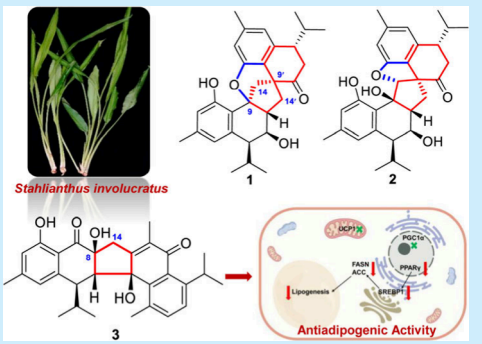

Cadinane-type sesquiterpenoid dimers (CSDs) represent structurally rare natural products,[1,2] with a limited number reported to date from higher plants—primarily within the families Asteraceae (*Artemisia*[3−6]), Malvaceae (*Gossypium*[2] and *Hibiscus*[7,8]), Zingiberaceae (*Curcuma*[9−12] and *Stahlianthus*[13−15]), Schisandraceae (*Schisandra*[16]), and Meliaceae (*Dysoxylum*[17]). Gossypol, the most extensively studied CSD, exhibits diverse pharmacological properties, including antifertility, antitumor, anti-HIV, and antimalarial activities.[18]

Stahlianthus involucratus ("*Wan Gai Pie*" in Dai medicine), a traditional herb from Xishuangbanna Dai Autonomous Prefecture (Yunnan, China), is used to treat traumatic injuries, rheumatic pain, bleeding disorders, and venomous bites.[19] Previous studies have demonstrated that its extracts are rich in cadinane sesquiterpenoids,[13−15,20] exhibiting anti-inflammatory, analgesic, antipyretic, and antioxidant activities.[21,22] Building upon our previous work on Zingiberaceae-derived bioactive compounds,[23−25] phytochemical investigation of *S. involucratus* led to the identification of three novel CSDs, distahlianins A–C (**1**–**3**) (Figure 1), displaying structurally unique and diverse carbon skeleton topologies. Compounds **1** and **2** feature a unique 5,6-spirocyclic core fused with different oxygenated heterocycles, forming complex 6/6/5/6/6/6 and 6/6/5/5/6/6 hexacyclic systems, respectively. Compound **3** displays an unprecedented dimeric architecture, where two monomeric subunits are interconnected via a central cyclopentane ring. Notably, another distinctive structural feature of **3** is the migration of the C14 methyl from C-9 to C-8 in the left monomer unit, establishing a structurally unique monomer motif. The putative biosynthetic pathways underlying the formation of **1**–**3** were also deduced. Bioassay revealed that **3** exhibited potent antiadipogenic activity with an EC_{50} value of 5.27 ± 0.75 μM, showing significant inhibition of triglyceride accumulation in differentiated 3T3-L1 adipocytes. Mechanistic studies revealed that **3** exerted its antiadipogenic effects through dose-dependent suppression of adipogenic regulators (SREBP1, PPARγ) and lipogenic enzymes (FASN, ACC), without affecting PGC1α/UCP1-mediated thermogenesis.

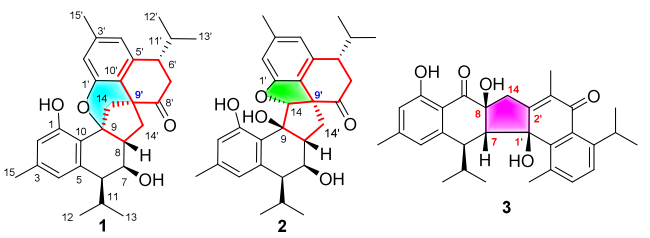

Figure 1. Structures of distahlianins A–C (**1**–**3**).

Distahlianin A (**1**) was isolated as colorless crystals from methanol with a specific rotation of $[\alpha]^{28}_{D}$ +170.7 (*c* 0.11 in MeOH). The HRESI-MS spectrum displayed an ion peak at *m*/*z* 461.2689 $[M+H]^+$ (calcd 461.2686), corresponding to the molecular formula $C_{30}H_{36}O_4$ with 13 degrees of unsaturation

Received: August 18, 2025
Revised: September 5, 2025
Accepted: September 16, 2025
Published: September 17, 2025

(DOUs). The IR data revealed the absorption bands for hydroxy (3406 cm^{-1}) and keto (1709 cm^{-1}) groups. The ^1H NMR spectrum (Table S1, Supporting Information) showed the characteristic proton signals for six methyls (including four secondary and two tertiary) and four aromatic methines. The ^{13}C NMR data (Table S1) and DEPT spectrum confirmed 30 carbon resonances, comprising one keto carbonyl, six methyls, three methylenes, ten methines (including one oxygenated and four aromatic), one oxygenated tertiary carbon, and nine quaternary carbons (including eight aromatic). Given the abundance of sesquiterpenoids in this plant,[13−15,20] compound **1** was hypothesized to be a sesquiterpenoid dimer.

The gross structure of **1** was unequivocally established by detailed elucidation of its 2D NMR correlations (Figure 2).

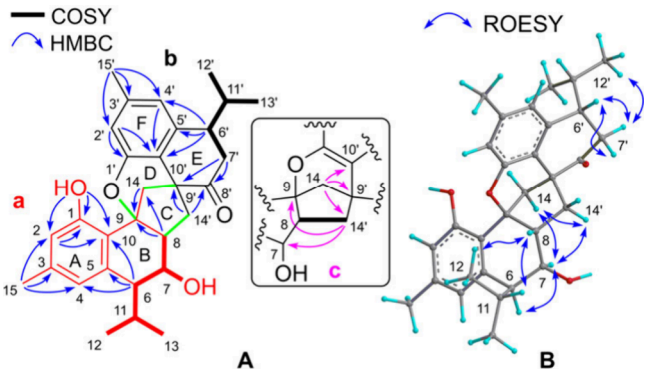

Figure 2. Selected $^1H-^1H$ COSY, HMBC (A), and ROESY (B) correlations of **1**.

The $^1H-^1H$ COSY correlations of H-8/H-7/H-6 (OH-7)/H-11/H_3-12 (H_3-13) and the key HMBC cross peaks of OH-1/C-1, C-2 and C-10; H-2/C-1 and C-10; H_3-15/C-2, C-3 and C-4; H-6/C-4, C-5 and C-10; H-8/C-9 (δ_C 87.9) and C-14; and H_2-14/C-9 (Figure 2A) identified the presence of a 1,7,9-trioxygenated cadinane sesquiterpenoid moiety (fragment **a**) in compound **1**. Similarly, fragment **b** (8′-oxocadinane sesquiterpenoid unit) was also deduced by the $^1H-^1H$ COSY correlations of H-7′/H-6′/H-11′/H_3-12′ (H_3-13′) and the HMBC correlations from H-2′ to C-1′ and C-10′; from H_3-15′ to C-2′, C-3′ and C-4′; from H-4′ to C-10′; from H-6′ to C-4′, C-5′ and C-10′; from H_2-7′ to C-8′ (δ_C 211.5) and C-9′; and from H_2-14′ to C-8′ and C-9′. The connectivity between fragments **a** and **b** was then fixed by the $^1H-^1H$ COSY correlation (H-8/H_2-14′) and HMBC correlation networks (H_2-14/C-9′, C-10′ and C-14′; and H_2-14′/C-7 and C-9), constructing a distinctive spiro[4.5]decane core via C14−C9′ and C14′−C8 carbon bridges (fragment **c**). The two monomeric units and the spirocyclic system accounted for 12 of the 13 DOUs, indicating the presence of an additional ring in compound **1**. The formation of an oxygen-containing heterocycle (ring C) via a C9−O−C1′ ether linkage was established by the diagnostic downfield shifts of C-9 and C-1′ (δ_C 153.9). Therefore, the complete structure of **1** was established as a novel CSD, featuring an unprecedented 5,6-spirocyclic core annulated with an oxygenated heterocycle to form a complex 6/6/5/6/6/6 ring system.

The relative configuration of compound **1** was primarily determined by ROESY experiment (Figure 2B). Key ROESY correlations of H-6/H-7, H-7/H-14α and H-14′α, H-14α/H-14′α, H-7′α/H_3-12′ arbitrarily defined their α-orientation, while the ROESY cross-peaks of H-8/H-11 and H_3-12, H-6′/H-7′α and H-7′β established the β-direction for H-8 and H-6′. The configurations at C-9 and C-9′ remained unassigned due to limited evidence. Single crystals of **1** suitable for X-ray diffraction were successfully obtained in methanol. The X-ray crystallographic analysis (CCDC number 2470166) unambiguously determined the absolute configuration of **1** to be 6*S*, 7*S*, 8*R*, 9*S*, 6′*S*, 9′*R* (Flack parameter = 0.15(9); Figure 3).

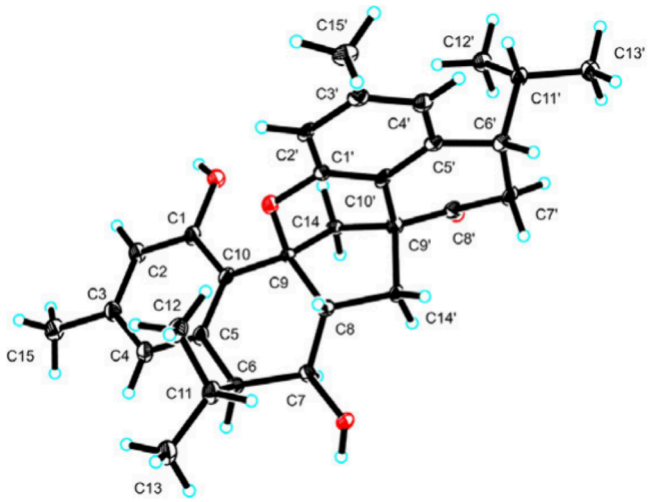

Figure 3. Single-crystal X-ray structure of **1** (displacement ellipsoids were drawn at the 35% probability level).

Distahlianin B (**2**) was assigned the molecular formula $C_{30}H_{36}O_5$, exhibiting a specific rotation of $[\alpha]^{20}_D$ −24.0 (*c* 0.07 in MeOH). The observed 16 mass unit increment relative to **1** suggests the introduction of an additional oxygen atom in its structure. Comprehensive analysis of the 1D NMR data (Table S1) and 2D NMR correlations (Figure S1) confirmed that **2** retains the characteristic 5,6-spirocyclic CSD framework present in **1**, but incorporates a modified oxygenated heterocyclic system. The diagnostic hydroxyl signal for OH-9 (δ_H 5.66, s), combined with the conclusive HMBC correlations from OH-9 to C-9, C-10 and C-14, established the presence of a free hydroxy group at C-9. Comprehensive analysis of the molecular formula, degrees of unsaturation, and the chemical shifts of C-14 (δ_C 98.3) and C-1′ (δ_C 158.1) confirmed the formation of an oxygen-containing five-membered heterocycle (ring C) through a C14−O−C1′ ether linkage. The gross structure of compound **2** was thus established as a spiro CSD incorporating a 6/6/5/5/6/6 polycyclic skeleton.

The relative configuration of **2** was determined by ROESY analysis (Figure S1). Key correlations of H-8/H-11, H_3-13 and H-14′β; OH-9/H-8, H-14 and H-14′β; H-6′/H-7′α and H-7′β; H-7′α/H_3-12′; and H-7/H-6 and H-14′α indicated the β-orientation for H-8, OH-9, H-14 and H-6′, and α-orientation for H-6 and H-7, respectively. The ROESY cross peaks of H-11′/H-14′α and H-14′β implied an *R**-configuration at C9′ in **2**. Apart from the oxygen-containing ring difference, the distinct C-9 configuration in compounds **1** and **2** likely accounts for their opposite optical rotations ($[\alpha]^{28}_D$ +170.7 for **1** and $[\alpha]^{20}_D$ −24.0 for **2**) and inverted Cotton effects (205−287 nm, Figures 4 and S2). The absolute configuration of **2** was finally established as 6*S*, 7*S*, 8*R*, 9*S*, 14*R*, 6′*S*, 9′*R* through TDDFT-based ECD calculations (Figure 4), which exhibited good agreement with the experimental spectrum.

https://doi.org/10.1021/acs.orglett.5c03471
Org. Lett. 2025, 27, 10843−10848

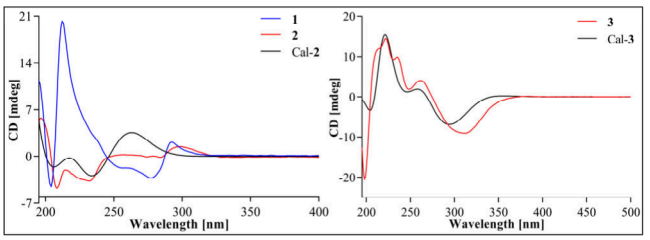

Figure 4. Experimental and calculated ECD spectra of **1**−**3**.

Distahlianin C (**3**) was assigned the molecular formula $C_{30}H_{34}O_5$ with 14 DOUs as determined by HRESI-MS analysis (ion peak observed at 497.2294 $[M+Na]^+$, calcd 497.2298) and ^{13}C NMR data. 1D NMR data (Table S1) and DEPT analysis identified a 30 carbon sesquiterpenoid dimer skeleton[13−15,20] comprising seven methyls (4 secondary, 3 tertiary), two keto carbonyls, one methylene, eight methines (including four olefinic), two oxygenated tertiary carbons, and ten olefinic quaternary carbons. The identified functional groups accounted for 9 of the 14 DOUs, with the remaining ones establishing a pentacyclic ring system for compound **3**.

The planar structure of **3** was elucidated through comprehensive 2D NMR spectroscopic analysis (Figure 5).

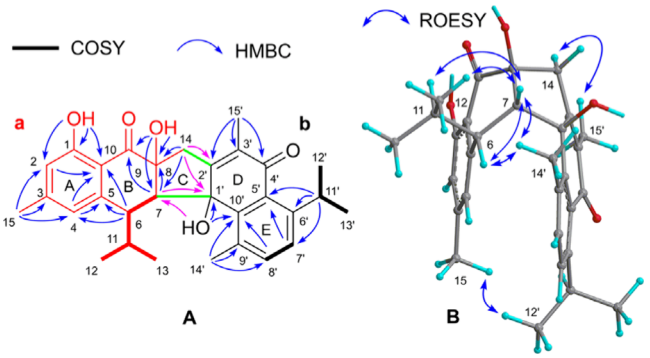

Figure 5. Selected $^1H-^1H$ COSY, HMBC (A), and ROESY (B) correlations of **3**.

The left sesquiterpenoid monomeric unit (fragment **a**) was deduced from the $^1H-^1H$ COSY correlations of H-7/H-6/H-11/H_3-12 (H_3-13) and the HMBC networks of OH-1/C-1, C-2 and C-10, H-2/C-10, H_3-15/C-2, C-3 and C-4, H-4/C-5 and C-10, H-6/C-4, C-5 and C-10, H-7/C-8 and C-9, OH-8/C-7, C-8 and C-9, and H_2-14/C-7 and C-8. Remarkably, fragment **a** undergoes an unprecedented C9→C8 migration of C-14 methyl relative to canonical cadinane framework, generating a novel carbon skeleton. In addition, the sesquiterpenoid fragment **b** (right side) was confirmed by the $^1H-^1H$ COSY cross peaks of H-7′/H-8′ and H_3-12′/H-11′/H_3-13′ and the HMBC correlations of OH-1′/C-1′, C-2′ and C-10′, H_3-15′/C-2′, C-3′ and C-4′, H-11′/C-5′, C-6′ and C-7′, H-7′/C-5′, H-8′/C-10′, and H_3-14′/C-8′, C-9′ and C-10′. The two units were ultimately linked via a cyclopentane ring (ring C) through key HMBC correlations of H-7/C-1′, H2−14/C-1′/C-2′, and OH-1′/C-7′, forming an unprecedented 6/6/5/6/6 pentacyclic CSD skeleton for **3**. The ROESY correlations of H-7/H-6, H-11, H_3-12 and H_3-14′; and H-6/H_3-14′ indicated that H-6 and H-7 were α- and β-directed, respectively. Furthermore, the coupling constant between H-6 and H-7 is 1.6 Hz, and the dihedral angle between them is approximately 70°, which is consistent with the Karplus equation. The β-configurations of OH-8 and OH-1′ were proposed based on the ROESY correlation of H_3-15 and H_3-12′ and spatial structure analysis. Quantum chemical NMR calculations at the PCM/mPW1PW91/6-31+G(d,p) level for all four diastereomers (Figure S3) further confirmed the 8*S**,1′*S**-**3** configuration through both optimal linear regression parameters (^{13}C: R^2 = 0.9994; ^1H: R^2 = 0.9892) and definitive DP4+ analysis (100% probability, Figures S5−S6). Finally, the absolute configuration of **3** was established as 6*R*, 7*S*, 8*S*, 1′*S* through comparative ECD analysis, demonstrating excellent agreement between calculated and experimental spectra (Figure 4).

The proposed biosynthetic routes for **1**−**3** are outlined in Schemes 1 and 2. Cadinane-type sesquiterpenoids, which are

Scheme 1. Plausible Biosynthetic Pathways for 1 and 2

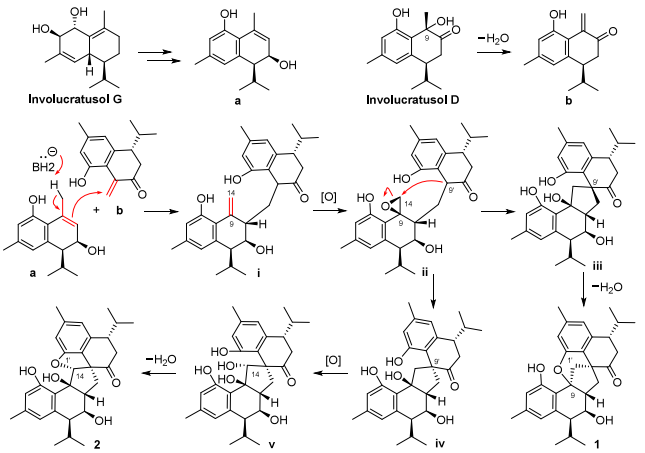

Scheme 2. Plausible Biosynthetic Pathways for 3

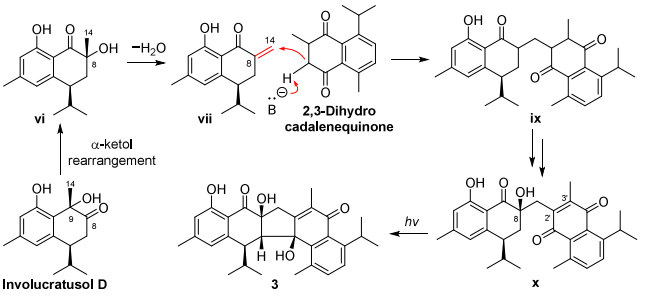

prevalent constituents of *S. involucratus*,[20] function as the monomeric building blocks for the formation of **1**−**3**. Monomers **a** and **b** are likely derived from the known compounds involucratusol G and D[20], respectively, which are characteristic constituents of *Stahlianthus involucratus*, and were thus proposed as their plausible biosynthetic precursors. Michael addition between **a** and **b** would afford intermediate **i**, which would subsequently be oxidized to epoxy intermediate **ii**. Epimeric intermediates **iii** and **iv** result from C-9′-initiated epoxy ring opening of **ii**, with **1** deriving from **iii** dehydration and **2** forming via C-14 oxidation of **iv** followed by C-1′−C-14 dehydration (Scheme 1). Regarding compound **3**, we initially postulated the C-14 methyl migration in its left fragment, proposing that involucratusol D undergoes an α-ketol rearrangement to generate the key intermediate **vi**.[26] The monomer **vii**, formed via dehydration of **vi**, undergoes Michael addition with 2,3-dihydrocadalenequinone[27] to yield dimeric intermediate **ix**. Sequential oxidation and hydration of **ix** then

https://doi.org/10.1021/acs.orglett.5c03471
Org. Lett. 2025, 27, 10843−10848

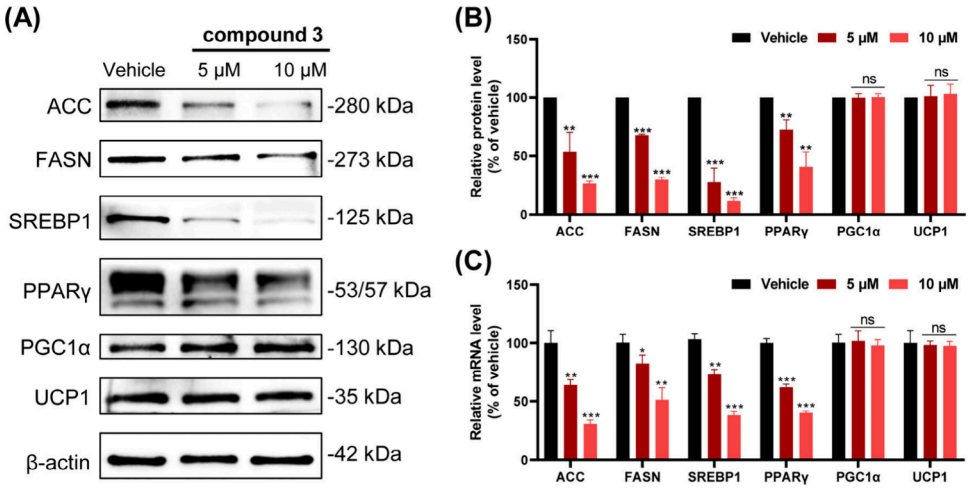

Figure 6. Dose-dependent effects of compound **3** (5 and 10 μM) on ACC, FASN, SREBP1, PPARγ, PGC1α and UCP1 expression at protein (A and B) and mRNA levels (C) (*P < 0.05, **P < 0.01, ***P < 0.001, NS = not statistically significant (P > 0.05)).

produce intermediate **x**, which ultimately converts to **3** through photoisomerization[28] (Scheme 2).

Antiadipogenic effects of compounds **1**−**3** were assessed using Oil Red O staining and triglyceride quantification in 3T3-L1 preadipocytes. All isolates reduced lipid accumulation at 20 μM with **3** exhibiting the strongest, dose-dependent inhibition (EC_{50} = 5.27 ± 0.75 μM, SI = 6.34) (Table S10 and Figure S7). During 3T3-L1 preadipocyte differentiation, core regulators peroxisome proliferator-activated receptor gamma (PPARγ, essential for adipogenesis[29−31]) and sterol regulatory element-binding protein (SREBP1, a master transcription factor in *de novo* lipogenesis[32]) are activated, driving triglyceride accumulation through enhanced activity of lipogenic enzymes-notably fatty acid synthase (FASN) for long-chain fatty acid synthesis and acetyl-CoA carboxylase (ACC) catalyzing acetyl-CoA to malonyl-CoA conversion. Parallelly, stimulation of adipose thermogenesis through the proliferator-activated receptor-γ coactivator-1α (PGC-1α)/uncoupling protein 1 (UCP1) signaling axis induces white adipose tissue browning and promotes beige adipocyte activation,[33−36] providing a complementary approach. Mechanistic studies revealed that **3** suppressed adipogenesis via downregulation of key adipogenic transcription factors (PPARγ and SREBP-1) and lipogenic enzymes (FASN and ACC), independent of PGC-1α mediated thermogenesis (Figure 6).

In summary, three unprecedented CSDs, distahlianins A−C (**1**−**3**), were isolated from *S. involucratus*. Structurally, compounds **1** and **2** contain a distinctive 5,6-spirocyclic system that annulated with oxygenated heterocycles to construct intricate 6/6/5/6/6/6 and 6/6/5/5/6/6 hexacyclic frameworks, respectively. Compound **3** represents the first reported cadinane dimer bridged by a cyclopentane ring. Significantly, **3** demonstrated potent antiadipogenic effect via selective lipogenesis suppression (PPARγ/SREBP1-FASN/ACC axis), unveiling a novel class of potential lipid-modulating natural products.

■ ASSOCIATED CONTENT

Data Availability Statement

The data underlying this study are available in the published article and its Supporting Information.

Supporting Information

The Supporting Information is available free of charge at https://pubs.acs.org/doi/10.1021/acs.orglett.5c03471.

1D NMR data of **1**−**3**, 2D NMR correlation analysis of **2**, X-ray crystallographic data of **1**, ECD calculation of **2**, NMR, DP4+ and ECD calculation of **3**, antiadipogenic effects of **1**−**3**, and the NMR, MS, CD and IR data for compounds **1**−**3** (PDF)

Accession Codes

Deposition Number 2470166 contains the supplementary crystallographic data for this paper. These data can be obtained free of charge via the joint Cambridge Crystallographic Data Centre (CCDC) and Fachinformationszentrum Karlsruhe Access Structures service.

■ AUTHOR INFORMATION

Corresponding Authors

Kai-Long Ji − *Key Laboratory of Tropical Plant Resources and Sustainable Use, Xishuangbanna Tropical Botanical Garden, Chinese Academy of Sciences, Kunming 650223 Yunnan, People's Republic of China*; orcid.org/0000-0003-4186-4086; Email: kl14ji@163.com

Gang Liang − *Key Laboratory of Tropical Plant Resources and Sustainable Use, Xishuangbanna Tropical Botanical Garden, Chinese Academy of Sciences, Kunming 650223 Yunnan, People's Republic of China*; Email: lianggang@xtbg.ac.cn

Yao-Yue Fan − *Shandong Laboratory of Yantai Drug Discovery, Bohai Rim Advanced Research Institute for Drug Discovery, Yantai 264117 Shandong, People's Republic of China; State Key Laboratory of Chemical Biology, Shanghai Institute of Materia Medica, Chinese Academy of Sciences, Shanghai 201203, People's Republic of China*; orcid.org/0000-0003-1387-202X; Email: s040500290@126.com

Authors

Yu-Han Chen − *Shandong Laboratory of Yantai Drug Discovery, Bohai Rim Advanced Research Institute for Drug Discovery, Yantai 264117 Shandong, People's Republic of China*

Qin-Qin Song − *Shandong Laboratory of Yantai Drug Discovery, Bohai Rim Advanced Research Institute for Drug*

https://doi.org/10.1021/acs.orglett.5c03471
Org. Lett. 2025, 27, 10843−10848

Discovery, Yantai 264117 Shandong, People's Republic of China

Xi-Yu Zheng − *Key Laboratory of Tropical Plant Resources and Sustainable Use, Xishuangbanna Tropical Botanical Garden, Chinese Academy of Sciences, Kunming 650223 Yunnan, People's Republic of China; School of Agriculture, Yunnan University, Kunming 650091 Yunnan, People's Republic of China*

Peng Sun − *Key Laboratory of Tropical Plant Resources and Sustainable Use, Xishuangbanna Tropical Botanical Garden, Chinese Academy of Sciences, Kunming 650223 Yunnan, People's Republic of China*

Jian-Mei Lu − *Key Laboratory of Tropical Plant Resources and Sustainable Use, Xishuangbanna Tropical Botanical Garden, Chinese Academy of Sciences, Kunming 650223 Yunnan, People's Republic of China*

Complete contact information is available at: https://pubs.acs.org/10.1021/acs.orglett.5c03471

Notes

The authors declare no competing financial interest.

■ ACKNOWLEDGMENTS

Financial support from Yunnan Fundamental Research Projects (No. 202501AT070248), Taishan Scholars Program (tsqn202408315), the Strategic Priority Research Program of the Chinese Academy of Sciences (XDB1060000), West Light Foundation of Chinese Academy of Sciences, and China Postdoctoral Science Foundation (2023T160677) is highly acknowledged. We are grateful to the Center for Gardening and Horticulture, Xishuangbanna Tropical Botanical Garden, Chinese Academy of Sciences, for supplying the plant samples used in this study.

■ REFERENCES

(1) Zhan, Z. J.; Ying, Y. M.; Ma, L. F.; Shan, W. G. Natural disesquiterpenoids. *Nat. Pro. Rep.* **2011**, *28*, 594−629.

(2) Ma, L. F.; Chen, Y. L.; Shan, W. G.; Zhan, Z. J. Natural disesquiterpenoids: an update. *Nat. Pro. Rep.* **2020**, *37*, 999−1030.

(3) He, X. F.; Li, Q. H.; Li, T. Z.; Ma, Y. B.; Dong, W.; Yang, K. X.; Geng, C. A.; Zhang, H. W.; Wang, Y.; Chen, J. J. Artemeriopolides A−D, two types of sesquiterpenoid dimers with rare carbon skeletons from Artemisia eriopoda and their antihepatoma cytotoxicity. *Org. Chem. Front.* **2023**, *10*, 2635−2641.

(4) He, X. F.; Ma, W. J.; Hu, J.; Li, T. Z.; Geng, C. A.; Ma, Y. B.; Wang, M. F.; Yang, K. X.; Zhang, X. M.; Chen, J. J. Diverse structures and antihepatoma effect of sesquiterpenoid dimers from *Artemisia eriopoda* by AKT/STAT signaling pathway. *Signal Transduct. Tar.* **2023**, *8*, 64.

(5) Wang, Y.; Li, T. Z.; Ma, Y. B.; Geng, C. A.; Wang, Y. C.; Chen, J. J. Artemordins A−S, cadinane-type sesquiterpenoid dimers from *Artemisia ordosica* and their antihepatoma activities. *Chin. J. Chem.* **2024**, *42*, 1493−1508.

(6) He, X. F.; Li, T. Z.; Ma, Y. B.; Wang, M. F.; Chen, J. J. Unusual cadinane-involved sesquiterpenoid dimers from *Artemisia annua* and their antihepatoma effect. *Phytochemistry* **2024**, *226*, 114216.

(7) Chen, D. L.; Ma, G. X.; Yang, E. L.; Yang, Y.; Wang, C. H.; Sun, Z. C.; Liang, H. Q.; Xu, X. D.; Wei, J. H. Cadinane-type sesquiterpenoid dimeric diastereomers hibisceusones A−C from infected stems of *Hibiscus tiliaceus* with cytotoxic activity against triple-negative breast cancer cells. *Bioorg. Chem.* **2022**, *127*, 105982.

(8) Chen, D. L.; Li, J. W.; Xu, X. D.; Sun, Z. C.; Yang, Y.; Xu, M. H.; Liang, H. Q.; Yang, J. S.; Meng, H.; Ma, G. X.; Wei, J. H. Plant-microbial interactions inspired the discovery of novel sesquiterpenoid dimeric skeletons of hidden natural products from *Hibiscus tiliaceus*. *Chin. Chem. Lett.* **2024**, *35*, 109451.

(9) Takahashi, M.; Koyano, T.; Kowithayakorn, T.; Hayashi, M.; Komiyama, K.; Ishibashi, M. Parviflorene A, a novel cytotoxic unsymmetrical sesquiterpene−dimer constituent from *Curcuma parviflora*. *Tetrahedron Lett.* **2003**, *44*, 2327−2329.

(10) Toume, K.; Takahashi, M.; Yamaguchi, K.; Koyano, T.; Kowithayakorn, T.; Hayashi, M.; Komiyama, K.; Ishibashi, M. Parviflorenes B−F, novel cytotoxic unsymmetrical sesquiterpene-dimers with three backbone skeletons from *Curcuma parviflora*. *Tetrahedron* **2004**, *60*, 10817−10824.

(11) Toume, K.; Sato, M.; Koyano, T.; Kowithayakorn, T.; Yamori, T.; Ishibashi, M. Cytotoxic dimeric sesquiterpenoids from *Curcuma parviflora*: isolation of three new parviflorenes and absolute stereochemistry of parviflorenes A, B, D, F, and G. *Tetrahedron* **2005**, *61*, 6700−6706.

(12) Ishibashi, M.; Tamaki, M.; Kumar Sadhu, S.; Ohtsuki, T.; Toume, K.; Koyano, T.; Kowithayakorn, T.; Hayashi, M.; Komiyama, K. Parviflorene J, a cytotoxic sesquiterpene dimer with a new rearranged skeleton from *Curcuma parviflora*. *Heterocycles* **2007**, *72*, 649−654.

(13) Li, Q. M.; Luo, J. G.; Zhao, H. J.; Yu, W. Y.; Wang, X. B.; Yang, M. H.; Luo, J.; Sun, H. B.; Chen, Y. C.; Guo, Q. L.; Kong, L. Y. Involudispirones A and B: sesterterpenes containing a dispiro ring from *Stahlianthus involucratus*. *Asian J. Org. Chem.* **2015**, *4*, 1366−1369.

(14) Li, Q. M.; Luo, J. G.; Zhang, Y. M.; Li, Z. R.; Wang, X. B.; Yang, M. H.; Luo, J.; Sun, H. B.; Chen, Y. J.; Kong, L. Y. Involucratustones A−C: unprecedented sesquiterpene dimers containing multiple contiguous quaternary carbons from *Stahlianthus involucratus*. *Chem.—Eur. J.* **2015**, *21*, 13206−13209.

(15) Li, Q. M.; Luo, J. G.; Wang, R. Z.; Wang, X. B.; Yang, M. H.; Luo, J.; Kong, L. Y. Involucratusins A−H: unusual cadinane dimers from *Stahlianthus involucratus* with multidrug resistance reversal activity. *Sci. Rep.* **2016**, *6*, 29744.

(16) He, T. B.; Yan, B. C.; Zhou, Y. F.; Sang, Y. Q.; Li, X. N.; Sun, H. D.; Wang, C.; Xue, X. S.; Puno, P. T. Discovery and bioinspired total syntheses of unprecedented sesquiterpenoid dimers unveiled bifurcating [4 + 2] cycloaddition and target differentiation of enantiomers. *Chem. Sci.* **2024**, *15*, 1260−1270.

(17) Naini, A. A.; Mayanti, T.; Harneti, D.; Darwati; Nurlelasari; Maharani, R.; Farabi, K.; Herlina, T.; Supratman, U.; Fajriah, S.; Kuncoro, H.; Azmi, M. N.; Shiono, Y.; Jungsuttiwong, S.; Chakthong, S. Sesquiterpenoids and sesquiterpenoid dimers from the stem bark of *Dysoxylum parasiticum* (osbeck) kosterm. *Phytochemistry* **2023**, *205*, 113477.

(18) Liu, Y. X.; Wang, L. L.; Zhao, L.; Zhang, Y. G. Structure, properties of gossypol and its derivatives−from physiological activities to drug discovery and drug design. *Nat. Pro. Rep.* **2022**, *39*, 1282−1304.

(19) Ma, X. J.; Zhang, L. X.; Lin, Y. F. *Zhongguo Daiyao Zhi* [*Chinese Dai Medicine Herbal*]; People's Medical Publishing House: Beijing, 2018; Vol. I, 36 pp.

(20) Li, Q. M.; Luo, J. G.; Zhang, Y. M.; Zhao, H. J.; Yang, M. H.; Kong, L. Y. Cadinane-type sesquiterpenoids from *Stahlianthus involucratus* and their absolute configurations. *Tetrahedron* **2016**, *72*, 6566−6571.

(21) Pingsusaen, P.; Kunanusorn, P.; Khonsung, P.; Chiranthanut, N.; Panthong, A.; Rujjanawate, C. Investigation of anti-inflammatory, antinociceptive and antipyretic activities of *Stahlianthus involucratus* rhizome ethanol extract. *J. Ethnopharmacol.* **2015**, *162*, 199−206.

(22) Li, W. K.; Wu, B. M.; Wang, Y.; Lin, Y.; An, L.; Zhang, G. F. The potential antioxidant activity and characterization of bioactive compounds of *Stahlianthus involucratus*. *BioMed. Res. Int.* **2021**, *2021*, 9490162.

(23) Ji, K. L.; Fan, Y. Y.; Ge, Z. P.; Sheng, L.; Xu, Y. K.; Gan, L. S.; Li, J. Y.; Yue, J. M. Maximumins A−D, rearranged labdane-type diterpenoids with four different carbon skeletons from *Amomum maximum*. *J. Org. Chem.* **2019**, *84*, 282−288.

(24) Ji, K. L.; Wu, M. Z.; Huang, C. Y.; GongPan, P. C.; Sun, P.; Sun, Y. L.; Li, J.; Xiao, C. F.; Xu, Y. K.; Fan, Q. F.; Hu, H. B.; Song, Q. S. *Alpinia hainanensis* rhizome extract ameliorates dextran sulfate sodium-induced ulcerative colitis: active ingredient investigation and evaluation. *J. Agric. Food Chem.* **2022**, *70*, 3989−3999.
(25) Wu, M. Z.; GongPan, P. C.; Dai, M. Y.; Sun, P.; Huang, T. P.; Xu, Y. K.; Xiao, C. F.; Li, J.; Sun, Y. L.; Ji, K. L. Dimeric styrylpyrones with stimulating GLP-1 secretion activities from *Alpinia kwangsiensis*. *Tetrahedron* **2022**, *120*, 132901.
(26) Benz, S.; Murkin, A. S. α-Ketol and α-iminol rearrangements in synthetic organic and biosynthetic reactions. *Beilstein J. Org. Chem.* **2021**, *17*, 2570−2584.
(27) Lien, L. T. N.; Guy, O. Cadalenequinone and dihydrocadalenequinone. Isolation from a Zingiberaceae and syntheses. *Bull. Soc. Chim. Fr.* **1983**, 112−114.
(28) Finucane, B. W.; Thomson, J. B. The photoisomerization of an 11-oxo-olean-12-ene. *J. Chem. Soc. D* **1969**, 380−380.
(29) Farmer, S. R. Regulation of PPARγ activity during adipogenesis. *Int. J. Obes.* **2005**, *29* (Suppl. 1), S13−S16.
(30) Angela, M.; Endo, Y.; Asou, H. K.; Yamamoto, T.; Tumes, D. J.; Tokuyama, H.; Yokote, K.; Nakayama, T. Fatty acid metabolic reprogramming via mTOR-mediated inductions of PPARγ directs early activation of T cells. *Nat. Commun.* **2016**, *7*, 13683.
(31) Lai, W.; Yu, L.; Deng, Y. PPARγ alleviates preeclampsia development by regulating lipid metabolism and ferroptosis. *Commun. Biol.* **2024**, *7*, 429.
(32) Zeng, H.; Qin, H.; Liao, M.; Zheng, E.; Luo, X.; Xiao, A.; Li, Y.; Chen, L.; Wei, L.; Zhao, L.; Ruan, X. Z.; Yang, P.; Chen, Y. CD36 promotes de novo lipogenesis in hepatocytes through INSIG2-dependent SREBP1 processing. *Mol. Metab.* **2022**, *57*, 101428.
(33) Je, J. Y.; Park, J. E.; Seo, Y.; Han, J. S. HM-chromanone inhibits adipogenesis by regulating adipogenic transcription factors and AMPK in 3T3-L1 adipocytes. *Eur. J. Pharmacol.* **2021**, *892*, 173689.
(34) Yan, M.; Audet-Walsh, É.; Manteghi, S.; Dufour, C. R.; Walker, B.; Baba, M.; St-Pierre, J.; Giguère, V.; Pause, A. Chronic AMPK activation via loss of FLCN induces functional beige adipose tissue through PGC-1α/ERRα. *Genes Dev.* **2016**, *30*, 1034−1046.
(35) Ringholm, S.; Knudsen, J. G.; Leick, L.; Lundgaard, A.; Nielsen, M. M.; Pilegaard, H. PGC-1α is required for exercise- and exercise training-induced UCP1 up-regulation in mouse white adipose tissue. *PloS One* **2013**, *8*, No. e64123.
(36) Chen, S.; Liu, X.; Peng, C.; Tan, C.; Sun, H.; Liu, H.; Zhang, Y.; Wu, P.; Cui, C.; Liu, C.; Yang, D.; Li, Z.; Lu, J.; Guan, J.; Ke, X.; Wang, R.; Bo, X.; Xu, X.; Han, J.; Liu, J. The phytochemical hyperforin triggers thermogenesis in adipose tissue via a Dlat-AMPK signaling axis to curb obesity. *Cell Metab.* **2021**, *33*, 565−580e7.

https://doi.org/10.1021/acs.orglett.5c03471
Org. Lett. 2025, 27, 10843−10848